Electronic and Optical Properties of Size-Controlled ZnO Nanoparticles Synthesized by a Facile Chemical Approach

Jindal, Shikha; Giripunje, Sushama Milind*[+]

Department of Applied Physics, Visvesvaraya National Institute of Technology, Nagpur, Maharashtra, INDIA

Kondawar, Subhash Baburao

Department of Physics, Rashtrasant Tukadoji Maharaj Nagpur University, Nagpur, Maharashtra, INDIA

ABSTRACT: *Facile low-temperature chemical route for the synthesis of ZnO nanoparticles is reported in this paper. Morphologically uniform and spherical shape with average particle size of 8.8 nm and wurtzite phase with the crystalline structure of as-synthesized ZnO nanoparticles were confirmed by X-Ray Diffraction (XRD), Scanning Electron Microscopy (SEM) and Transmission Electron Microscopy (TEM). The optical properties of ZnO nanoparticles were analyzed by UltraViolet Visible (UV-Vis) absorption and PhotoLuminescence (PL). The as-synthesized ZnO nanoparticles showed orange light-emitting properties when excited at 400 nm due to the well overlapping of electron and hole wave function across the compatible size of the particle of ZnO and the optical energy band gap of 3.5 eV due to quantum confinement. X-ray Photoelectron Spectroscopy (XPS) and Ultraviolet Photoelectron Spectroscopy (UPS) were used for the elemental, molecular and energetic information of ZnO nanoparticles. UPS analysis depicted the energy level position of ZnO nanoparticles whereas XPS spectra showed the presence of constitute elementals with the stoichiometric atomic % of Zn and O. The elemental composition was also confirmed by the EDS analysis. The significant Raman shifts for as-synthesized ZnO nanoparticles in the typical Raman-active modes of vibration assigned to the wurtzite crystal nanostructure of ZnO.*

KEYWORDS: *Zinc oxide; Nanoparticles; XPS; UPS; Raman spectra.*

INTRODUCTION

From the past few decades, nanostructured materials have been widely used in various fields such as material science, physical, chemical, and biological applications. It has an immense interest in the form of nanoparticles, nanorods, nanotubes, thin films due to its size-dependent quantum confinement effect. Owing to its tremendous properties, a variety of binary, ternary, quaternary semiconductor nanoparticles have developed to introduce these materials in different applications. Currently, the binary oxides, sulfides, selenides, tellurides semiconductors have been deployed in nanostructured devices. Among these, oxide semiconductor nanoparticles have attracted more attention due to some reasons; that it does not require the inert atmosphere to synthesize as well as to preserve the material. From this perspective, oxide nanoparticles have been easily arranged in electronics,

* *To whom correspondence should be addressed.*

+ *E-mail: smgiripunje@phy.vnit.ac.in*

1021-9986/2019/5/11-20 10/$/6.00

energy storage, photocatalysis, sensors and memory devices [1-9]. ZnO, an II-VI oxide binary semiconductor is a wide bandgap material of 3.37 eV. It has high electron mobility and is highly transparent [10]. Besides, it exists in the wurtzite and zinc blende phases but the wurtzite phase is stable at room temperature. Due to its intense optical and electrical properties, ZnO has been widely used in various fields such as solar cells, light-emitting diodes, sensors, photocatalysis, etc [11-17]. Recently, ZnO nanostructures have been used in electronic applications in various forms such as nanodisks, nanorods, nanowalls, nanocombs and nanorings[18-22]. *Hussain et al.* have reported the synthesis of ZnO nanodisk for gas sensing applications [18]. However, the ZnO nanorods for electrochemical sensors were studied by *Molaakbari et al.* [20]. Thus, ZnO has been synthesized by various processes which include hydrothermal process, thermal treatment process, microwave irradiated process and laser ablation method [23-26].

In this article, we have reported the facile synthesis of ZnO nanoparticles by wet chemical methods. In this process, we have used abundant precursors like zinc acetate and potassium hydroxide. Its structural, optical and vibrational properties have been studied. Moreover, we have analyzed the UPS spectra to investigate the electronic energy levels. Hence, the work function, valence band, and conduction band have been measured from UPS results to analyze the feasibility of material in various electronic devices such as solar cells and light-emitting diodes. This investigation concludes that the ZnO nanoparticles can be utilized as a window layer in various low bandgap semiconductor material devices.

EXPERIMENTAL SECTION

Materials

Zinc acetate ($Zn(CH_3COO)_2.2H_2O$), potassium hydroxide (KOH) and ethanol were used as precursors. All the chemicals were of analytical grade and have been used without further purification.

Synthesis of ZnO nanoparticles

ZnO nanoparticles were prepared by a simple and facile chemical method. In a typical synthesis, an aqueous solution of zinc acetate was prepared by adding 0.1 M ($Zn(CH_3COO)_2.2H_2O$)in the methanol by stirring for 5 min. Another solution of potassium hydroxide was also prepared separately by mixing of 0.4 M KOH in the methanol by stirring. After dissolving the solutions, an aqueous solution of potassium hydroxide was added in the zinc acetate aqueous solution dropwise with continuous stirring. The mixture was allowed to stir for 2 hrs 30 min at 60°C. Then after, the mixture was kept to cool down at room temperature. The mixed solution was centrifuged at 10,000 rpm for 5 min. The precipitated particles were washed several times with methanol to remove the remnant impurities. Subsequently, as-prepared particles were dispersed in chloroform. Finally, ZnO particles were dried in a vacuum at room temperature.

Characterization

X-Ray Diffraction (XRD) spectra were recorded by using Rigaku, Smart Lab X-R Diffractometer in the 2θ range of 20–80° with the Cu Kα radiation. Scanning electron microscopy (SEM) images were carried out by Ultra 55 ZEISS a microscope and Energy Dispersive Spectrum (EDS) was analyzed by X-MAX from Oxford instruments connected with SEM. Transmission Electron Microscopy (TEM) was analyzed by Technai G^2 20 microscope at the operating voltage of 200 kV. The TEM sample preparation was done by dispersing the sample in methanol and coated on a carbon-coated copper grid. SAED pattern was collected to confirm the crystallinity of the sample. The optical absorption spectra were performed on Shimadzu, UV-3600 UV-Vis-NIR spectrophotometer. PhotoLuminescence (PL) spectra was recorded by JASCO Spectroflurometer FP-8200. X-ray Photoelectron Spectroscopy (XPS) and Ultraviolet Photoelectron Spectroscopy (UPS) spectra were recorded by Kratos Axis Ultra DLD. XPS spectra were collected by using the Al K-Alpha radiation (hυ= 1486.6 eV) source at the accelerating voltage of 13kV and UPS spectra was measured using a He (I) laser source. Raman analysis was carried out using Horiba Jobin YVON Lab RAM HR spectrophotometer with an excitation wavelength of 532 nm.

RESULTS AND DISCUSSION

Reaction stoichiometry

The hydrolysis of zinc acetate with KOH in the solution provides the formation of ZnO particles. Due to the heating, zinc acetate undergoes hydrolysis forming

acetate ions and zinc ions. The intermediate product, zinc hydroxide was formed in the presence of OH^- ions of ethanol acetate as it forms bonds with zinc ions and it get easily transformed into ZnO. The overall chemical reaction to synthesize ZnO nanoparticles is stated as follow in Eq. (1):

$$Zn(CH_3COO)_2.2H_2O + 2KOH \longrightarrow ZnO + 2CH_3COOK + 3H_2O \quad (1)$$

Structural and morphological studies

The structural analysis of ZnO nanoparticles was investigated by XRD. Fig. 1 depicts the XRD of ZnO nanoparticles and ICSD: 01-080-0075 of hexagonal ZnO. The spectra illustrate the diffraction peaks at 2θ values 31.69°, 34.35°, 36.20°, 47.48°, 56.54°, 62.80°, 67.92° corresponding to (100), (002), (101), (102), (110), (103), (112) crystal planes of hexagonal ZnO, respectively. These results are well-matched with the ICSD file no. 01-080-0075. XRD spectra confirm the wurtzite phase of ZnO nanoparticles. Moreover, the broadening of peaks shows the quantum confinement effect in nanoparticles. The crystallite size of ZnO was determined by using Debye Scherrer's formula and was found to be 8.9 nm.

The surface morphology of nanoparticles was envisaged by SEM. Fig. 2a,b shows the spherical particles of ZnO with an average particle size of 10.23 nm. Furthermore, the images of SEM show the uniform distribution of particles. The elemental composition of ZnO was analyzed by EDS. EDS spectra of ZnO (Fig. 2c) confirms the presence of Zn and O with atomic weight % of Zn and O are 45.35% and 54.65%, respectively. These results are summarized in Table 1.

The structure and morphology of ZnO nanoparticles were analyzed by TEM analysis. The low and high-resolution TEM images of ZnO nanoparticles are shown in Fig. 3a,c respectively. These images show the uniformly distributed spherical particles. Fig. 3b shows the particle size distribution of ZnO. Hence, the particle size of ZnO was determined to be 8.8 ± 1.5 nm. The inset of Fig. 3a shows the SAED pattern of ZnO. Consequently, these diffraction rings correspond to the (100), (002), (101), (102), (110), (103), (112) plane of ZnO. The continuous diffused rings confirm the polycrystalline nature of nanoparticles and show

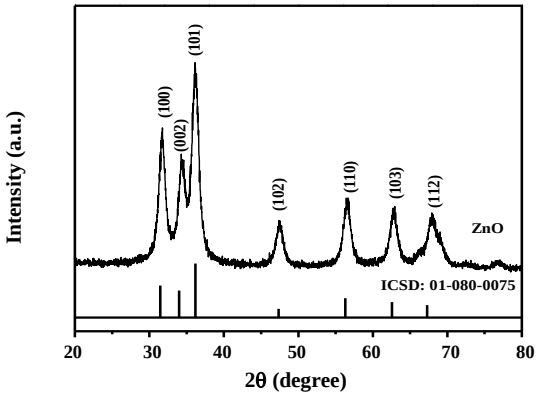

Fig. 1: XRD patterns of ZnO nanoparticles and ICSD: 01-080-0075.

the formation of small-sized particles. These results are consistent with the XRD results.

Optical studies

UV-Visible absorption spectra were recorded to investigate the bandgap of ZnO nanoparticles. Fig. 4a shows the absorbance spectra of ZnO nanoparticles corresponding to the wavelength. The absorption band edge of ZnO was observed at 357 nm. However, the optical band gap of ZnO was calculated from the plot of $(\alpha h\nu)^2$ versus hν (Fig. 4b), by using the Tauc's relation [27] as equation (2):

$$(\alpha h\nu)^n = c(h\nu - E_g) \quad (2)$$

Where hν is the photon energy, α is the absorption coefficient, c is constant relative to the material. The parameter n is associated with the different types of electronic transitions: n=2, 1/2, 2/3 or 3 for the direct–allowed, indirect–allowed, direct–forbidden and indirect–forbidden transitions, respectively. ZnO is a direct bandgap material. Thus the value of n is chosen to be 2. To calculate the bandgap of ZnO nanoparticles, the linear portion of the $(\alpha h\nu)^2$ was extrapolated to the hν=0 and the corresponding energy band gap was found to be 3.5 eV.

Fig. 4c depicts the excitation dependent PL emission spectra. The emission spectra were recorded at different excitation wavelengths (λ_{ex}) namely; 360, 380, 400, 420, 440 nm. Consequently, the visible emission peaks were observed in the spectra. The emission in the visible region was due to the electron-hole recombination

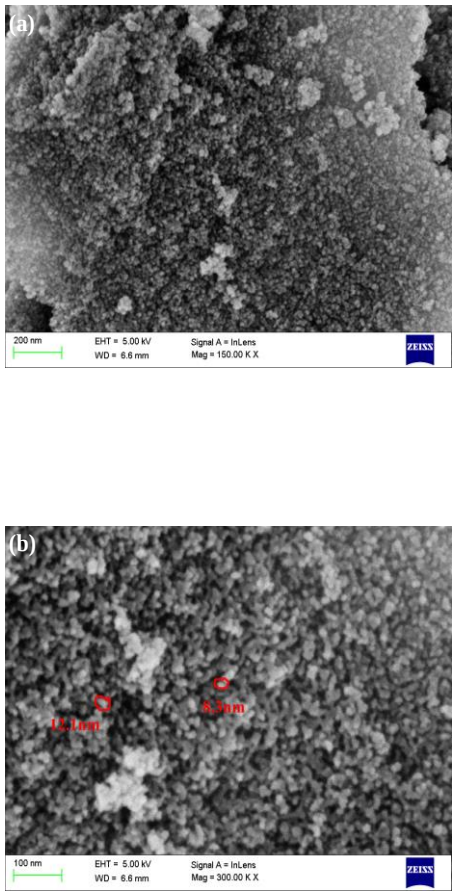

Fig. 2: (a, b) Low and high-resolution SEM images of ZnO sample and (c) EDS spectra of ZnO sample.

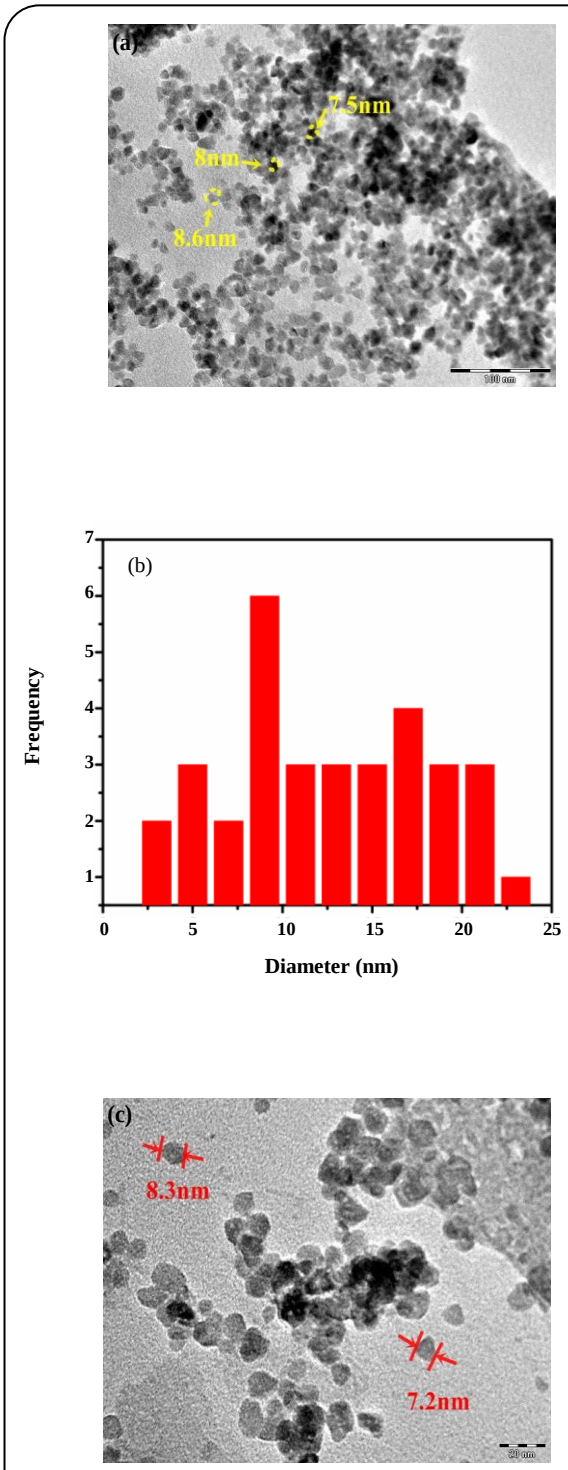

Fig. 3: (a, c) Low and high-resolution TEM images of ZnO sample, inset is the SAED image of the sample and (b) The particle size distribution of ZnO.

Table 1: EDS spectra of ZnO nanoparticles.

Element	Atomic %
Zn	45.35
O	54.65

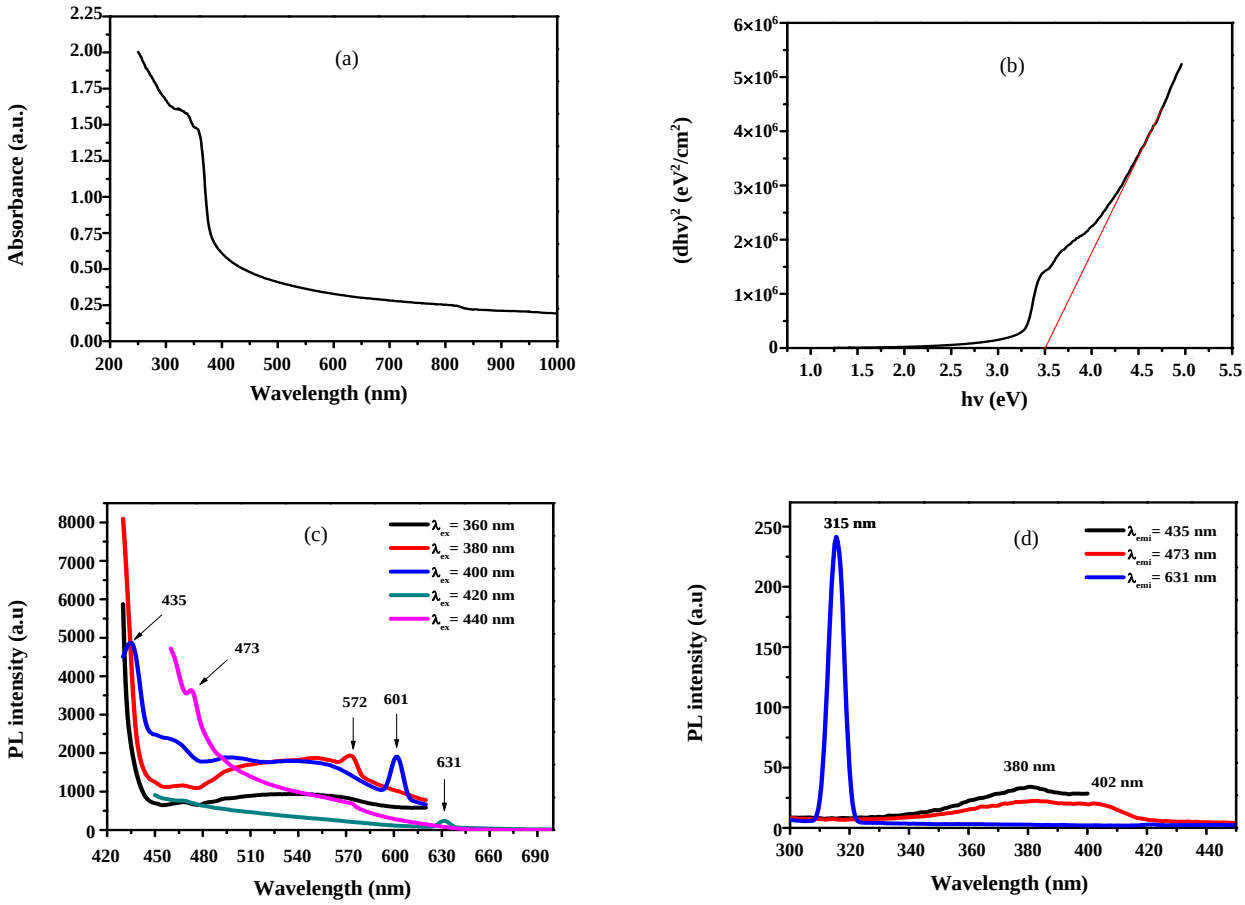

Fig. 4: (a) UV-Visible spectra of ZnO nanoparticles and (b) Plot of $(\alpha h\nu)^2$ vs hv, (c) PL emission spectra of ZnO nanoparticles and (d) PL excitation spectra of ZnO nanoparticles.

at deep levels which was caused by intrinsic defects and surface defect. However, the higher emission intensity was observed in the orange region at 601 nm when the ZnO particles were excited at 400 nm wavelength. This happens due to the overlapping of electron and hole wave function caused by the quantum confinement effect. The emission wavelength is shifted to the red region at 631 nm with a decrease in intensity upon excitation of 420 nm. The spectra also show emission in the blue region which was shifted at different excitation wavelengths. As a consequence, blue emissions occurred preferentially at near band edge excitation and visible emissions occurred at the higher band-edge excitation wavelength. The spectra reveal the shift in emission towards higher wavelength upon excitation of different wavelengths [28].

PLE spectra of blue and red regions have been recorded at emission wavelengths (λ_{emi}) from 435 to 631 nm as shown in Fig. 4d. In the case of red region emission, the PLE spectra depict the peak occur at 315 nm confirms the excitation in near UV region indicates that the excitation energy is larger than the bandgap. For the blue emission, PLE spectra depict the peak occurred

at 380 nm predicts the near band gap excitation. In violet region emission, the peak was shifted to 402 nm along with the tail covers the violet region.

XPS analysis

The elemental composition and oxidation states were investigated by XPS spectroscopy. The XPS survey spectrum of ZnO nanoparticles is shown in Fig. 5a. The spectra confirm the existence of Zn, O elements in the sample. Fig. 5b illustrates the high-resolution XPS spectra of Zn 2p element. The symmetrical spectra of Zn demonstrate the doublet peak at binding energies of 1022.4 and 1045.5 eV are associated to the Zn $2p_{3/2}$ and $2p_{1/2}$, respectively. Thus, these peaks are consistent with the oxidation state of Zn^{2+} [29]. The high-resolution XPS spectra of O element is depicted in Fig. 5c. Noteworthy, the asymmetrical spectra of O indicates the two deconvoluted peaks at binding energies of 531.3 eV and 532.7 eV by peak fitting. The peak at 531.3 eV attributed to the O^{2-} oxidation state of the wurtzite lattice of ZnO (O_L) and the peak present at 532.7 eV corresponds to the O vacancies or defects in the lattice (O_V) [30]. These XPS results are consistent with the values reported in the literature of ZnO material [31-33].

Furthermore, the quantitative analysis of XPS is represented in Table 2. The stoichiometry of ZnO confirms with the atomic concentration of Zn and O to be 49.13% and 50.87%, respectively. These results are relevant to the EDS results.

UPS analysis

UPS spectra were carried out to determine the energy levels and work function of ZnO nanoparticles. The recorded spectrum is shown in Fig.6. From the spectra, valence band onset (E_{onset}) and secondary electron cut-off (E_{cutoff}) was calculated to be 2.99 eV and 19.26 eV, respectively. The work function was determined by the difference between the incident photon energy and secondary electron cut-off as represented in the Equation (3):

$$\varnothing = h\nu - E_{cutoff} \quad (3)$$

The formalism to calculate the Valence Band Maxima (VBM) is given in Equation (4) [34]:

$$VBM = h\nu - \left(E_{cutoff} - E_{onset}\right) \quad (4)$$

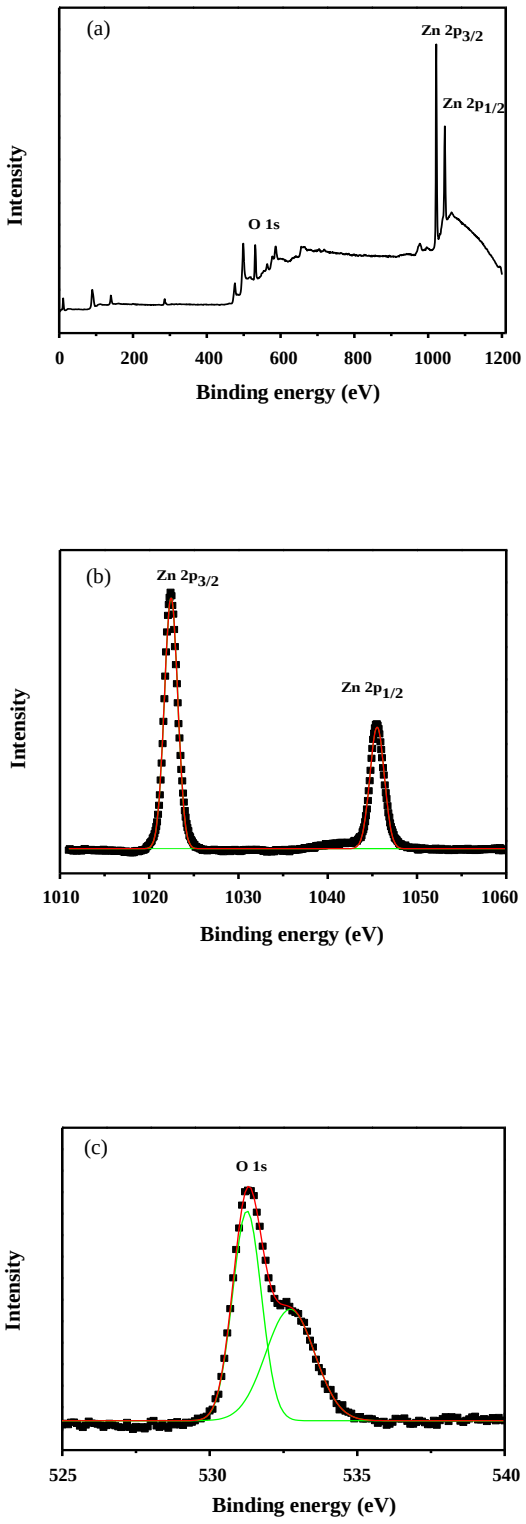

Fig. 5: (a) XPS survey spectra; and high-resolution spectra of (b) Zn 2p, (c) O 1s of ZnO nanoparticles.

Table 2: XPS determined surface elemental composition of ZnO nanoparticles.

Element	FWHM (eV)	Atomic conc. (%)
Zn 2p	2.868	49.13
O 1s	3.359	50.87

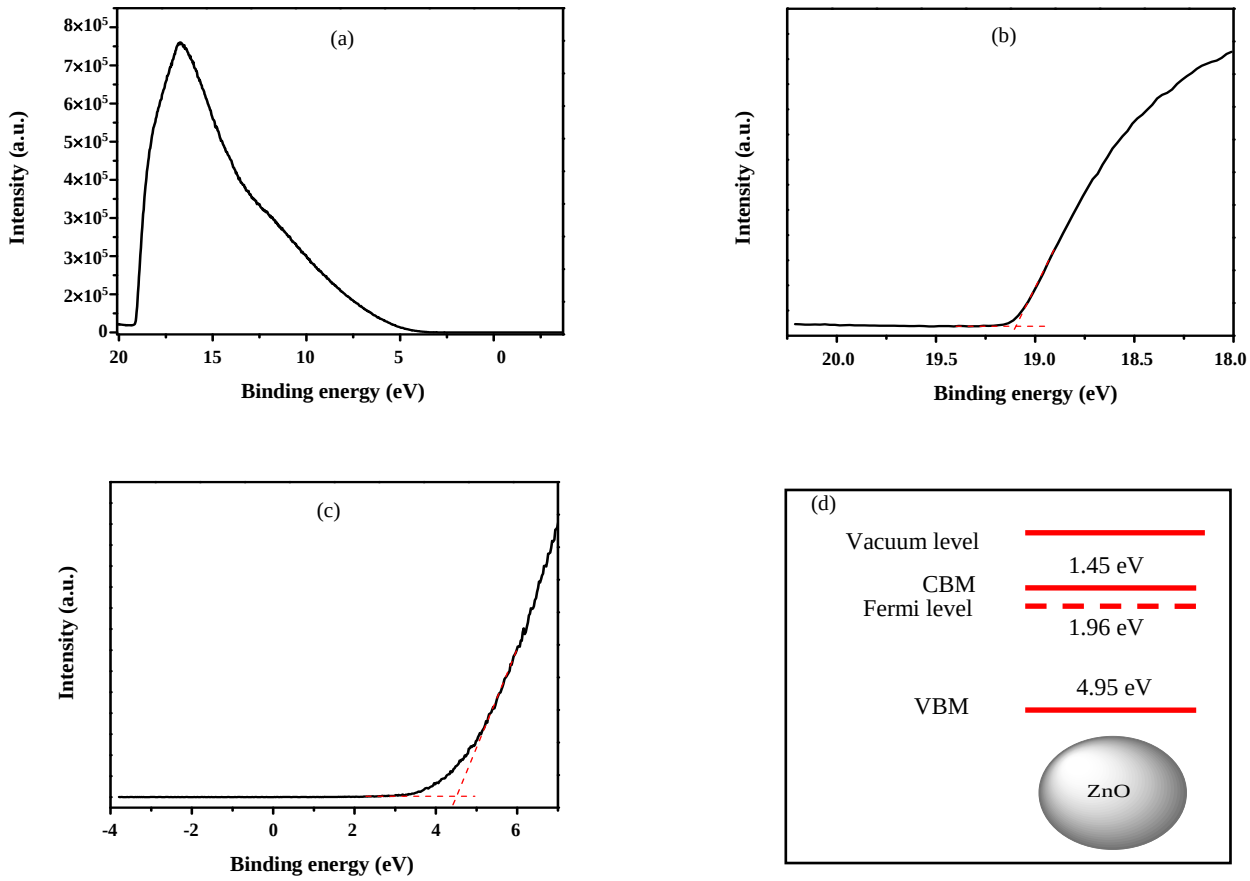

Fig. 6: (a) UPS spectra of ZnO nanoparticles, (b) Secondary edge region of ZnO nanoparticles (c) Valence band onset region of UPS spectra of ZnO nanoparticles and (d) Energy levels of ZnO nanoparticles.

By using the incident energy, hν=21.22 eV (He1 laser source); the calculated work function and valence band maxima were found to be 1.96 eV and 4.95 eV, respectively. The optical absorption bandgap was determined to be 3.5 eV as calculated from the UV- visible absorbance spectra. Consequently, the Conduction Band Minima (CBM) was calculated to be 1.45. The investigated data is summarized in Table 3.

Vibrational properties

Fig. 7 represents Raman spectra of ZnO nanoparticles. Raman spectrum of ZnO depicts five prominent peaks at 419, 439, 514, 669 and 936 cm^{-1}. The Raman peak at 419 cm^{-1} is attributed to be E1 (TO) vibrational mode [35]. Also, the sharp peak at 439 cm^{-1} corresponds to the E2 (high) phonon mode of ZnO [36, 37]. The peak centered at 514 cm^{-1} may be assigned to the A1 (LA) model [35]. The two phonon vibrational modes A (LO) + E (low) was assigned to Raman peak at 669 cm^{-1} [31]. Along with this, the strong and sharp peak at 936 cm^{-1} is present due to the C-C symmetric stretching vibrations [38].

CONCLUSIONS

A simple wet chemical method has been utilized to fabricate the ZnO nanoparticles. XRD spectra confirm the formation of wurtzite phase of ZnO with average

Table 3: Energy band information calculated from UPS and UV-visible absorption spectra.

Material	Secondary cut-off (eV)	Work function	Valence band onset (eV)	Valence band maximum (eV)	Band gap (eV)	Conduction band minima (eV)
ZnO	19.26	1.96	2.99	4.95	3.5	1.45

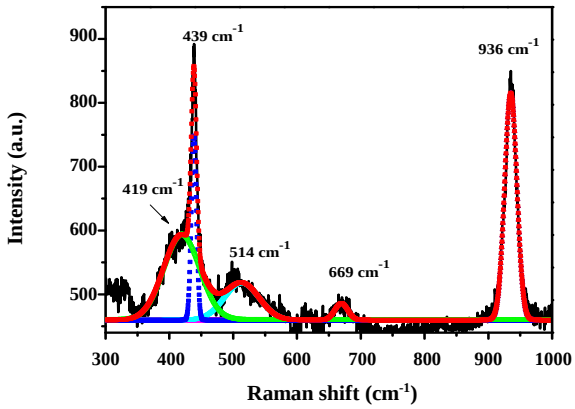

Fig. 7: Raman spectra of ZnO nanoparticles.

the particle size of 8.8 nm. SEM and TEM analysis reveals the spherical and uniform size particles. These results are consistent with XRD results. EDS and the quantitative XPS analysis show the stoichiometry in atomic % of Zn and O elements. UPS spectra were recorded to analyze the energy levels of particles. Raman spectra confirm the presence of the ZnO vibrational phase.

Acknowledgments

Authors are thankful towards CeNSE, Indian Institute of Science, Bangalore, funded by the Department of Electronics and Information Technology (DeitY), Govt. of India for carrying out the characterization facilities. We would also like to express our sincere thanks to Dr. N. P. Lalla, UGC-DAE-CSR, and Indore for providing the TEM facility.

Received : Oct. 18, 2017 ; Accepted : Jul. 16, 2018

REFERENCES

[1] Sutka A., Gross K.A., Spinel Ferrite Oxide Semiconductor Gas Sensors, *Sensors and Actuators B: Chemical*, **222**: 95-105 (2016).

[2] Petti L., Munzenrieder N., Vogt C., Faber H., Buthe L., Cantarella G., Bottacchi F., Anthopoulos T.D., Troster G., Metal Oxide Semiconductor Thin-Film Transistors for Flexible Electronics, *Applied Physics Reviews*, **3**(2): 021303 (2016).

[3] Yu X., Marks T.J., Facchetti A., Metal Oxides for Optoelectronic Applications, *Nat Mater*, **15**(4): 383-96 (2016).

[4] Meyer J., Hamwi S., Kröger M., Kowalsky W., Riedl T., Kahn A., Transition Metal Oxides for Organic Electronics: Energetics, Device Physics and Applications, *Adv. Mater.*, (2012). DOI: 10.1002/adma.201201630.

[5] Yang P., Sun P., Mai W., Electrochromic Energy Storage Devices, *Materials Today*, **19**(7): 394-402 (2016).

[6] Lukatskaya M.R., Dunn B., Gogotsi Y., Multidimensional Materials and Device Architectures for Future Hybrid Energy Storage, *Nat Commun*, **7**: 12647 (2016).

[7] Djurisic A.B., Leung Y.H., Ching Ng A.M., Strategies for Improving the Efficiency of Semiconductor Metal Oxide Photocatalysis, *Materials Horizons*, **1**(4): 400-410 (2014).

[8] Khan M.M., Adil S.F., Al-Mayouf A., Metal Oxides as Photocatalysts, *Journal of Saudi Chemical Society*, **19**(5): 462-464 (2015).

[9] Kundu S., Rao Gollu S., Sharma R., Halder N.N., Biswas P., Banerji P., Gupta D., GaAs Metal-Oxide-Semiconductor Based Nonvolatile Memory Devices Embedded with ZnO Quantum Dots, *Journal of Applied Physics*, **114**(8): 084509 (2013).

[10] El-Desoky M.M., Ali M.A., Afifi G., Imam H., Annealing Effects on the Structural and Optical Properties of Growth ZnO Thin Films Fabricated by Pulsed Laser Deposition (PLD), *Journal of Materials Science: Materials in Electronics*, **25**(11): 5071-5077 (2014).

[11] Tseng Z.L., Chiang C.H., Wu C.G., Surface Engineering of ZnO Thin Film for High Efficiency Planar Perovskite Solar Cells, *Sci. Rep.*, **5**: 13211 (2015).

[12] Apostoluk A., Zhu Y., Masenelli B., Delaunay J.-J., Sibinski M., Znajdek K., Focsa A., Kaliszewska I., Improvement of the Solar Cell Efficiency by the ZnO Nanoparticle Layer *via* the Down-Shifting Effect, *Microelectronic Engineering*, **127**: 51-56 (2014).

[13] Wu Z., Song T., Xia Z., Wei H., Sun B., Enhanced Performance of Polymer Solar Cell with ZnO Nanoparticle Electron Transporting Layer Passivated by in Situ Cross-Linked Three-Dimensional Polymer Network, *Nanotechnology*, **24**(48): 484012 (2013).

[14] Huang C.-Y., Lai J.-H., Efficient Polymer Light-Emitting Diodes with ZnO Nanoparticles and Interpretation of Observed Sub-Bandgap Turn-on Phenomenon, *Organic Electronics*, **32**: 244-249 (2016).

[15] Zheng Z.Q., Yao J.D., Wang B., Yang G.W., Light-Controlling, Flexible and Transparent Ethanol Gas Sensor Based on ZnO Nanoparticles for Wearable Devices, *Sci Rep.*, **5**: 11070 (2015).

[16] Torres-Hernandez J.R., Ramirez-Morales E., Rojas-Blanco L., Pantoja-Enriquez J., Oskam G., Paraguay-Delgado F., Escobar-Morales B., Acosta-Alejandro M., Diaz-Flores L.L., Perez-Hernandez G., Structural, Optical and Photocatalytic Properties of ZnO Nanoparticles Modified with Cu, *Materials Science in Semiconductor Processing*, **37**: 87-92 (2015).

[17] Hirschmann J., Faber H., Halik M., Concept of a Thin Film Memory Transistor Based on ZnO Nanoparticles Insulated by a Ligand Shell, *Nanoscale*, **4**(2): 444-7 (2012).

[18] Hussain S., Liu T., Kashif M., Miao B., Lin L., Zeng W., Rashad M., Peng X., Pan F., Preparation of ZnO Nanodisks Using Hydrothermal Method and Sensing to Reductive Gases, *Journal of Materials Science: Materials in Electronics*, **25**(11): 4725-4729 (2014).

[19] Molaakbari E., Mostafavi A., Beitollahi H., Alizadeh R., Synthesis of ZnO Nanorods and Their Application in the Construction of a Nanostructure-Based Electrochemical Sensor for Determination of Levodopa in the Presence of Carbidopa, *Analyst*, **139**(17): 4356-64 (2014).

[20] Comjani F.F., Willer U., Kontermann S., Schade W., Synthesis of ZnO Nanowalls and Nanocombs by Vapor–Liquid–Solid Method, *Physica Status Solidi (a)*, **210**(10): 2219-2223(2013).

[21] Schlur L., Carton A., Leveque P., Guillon D., Pourroy G., Optimization of a New ZnO Nanorods Hydrothermal Synthesis Method for Solid State Dye Sensitized Solar Cells Applications, *The Journal of Physical Chemistry C*, **117**(6): 2993-3001 (2013).

[22] Li C., Lin Y., Li F., Zhu L., Sun D., Shen L., Chen Y., Ruan S., Hexagonal ZnO Nanorings: Synthesis, Formation Mechanism and Trimethylamine Sensing Properties, *RSC Adv.*, **5**(98): 80561-80567 (2015).

[23] Bharti D.B., Bharati A.V., Synthesis of ZnO Nanoparticles Using a Hydrothermal Method and a Study Its Optical Activity, Luminescence (2016).

[24] Lee P., Saion E., Al-Hada N., Soltani N., A Simple Up-Scalable Thermal Treatment Method for Synthesis of ZnO Nanoparticles, *Metals*, **5**(4): 2383-2392 (2015).

[25] Barreto G.P., Morales G., Quintanilla M.L.L., Microwave Assisted Synthesis of ZnO Nanoparticles: Effect of Precursor Reagents, Temperature, Irradiation Time, and Additives on Nano-ZnO Morphology Development, *Journal of Materials*, **2013**: 1-11 (2013).

[26] Ismail R.A., Ali A.K., Ismail M.M., Hassoon K.I., Preparation and Characterization of Colloidal ZnO Nanoparticles Using Nanosecond Laser Ablation in Water, *Applied Nanoscience*, **1**(1): 45-49 (2011).

[27] Mathur V., Rathore K.S., Sharma K., Evaluation of Energy Band Gap, Thermal Conductivity, Phase Transition Temperature and Elastic Response of PS/CdS Semiconducting Optical Nanocomposite, *World Journal of Nano Science and Engineering*, **03**(03): 93-99 (2013).

[28] Zeng H., Duan G., Li Y., Yang S., Xu X., Cai W., Blue Luminescence of ZnO Nanoparticles Based on Non-Equilibrium Processes: Defect Origins and Emission Controls, *Advanced Functional Materials*, **20**(4): 561-572 (2010).

[29] Morozov I.G., Belousova O.V., Ortega D., Mafina M.K., Kuznetcov M.V., Structural, Optical, XPS and Magnetic Properties of Zn Particles Capped by ZnO Nanoparticles, *Journal of Alloys and Compounds*, **633**: 237-245 (2015).

[30] Zhang X., Qin J., Xue Y., Yu P., Zhang B., Wang L., Liu R., Effect of Aspect Ratio and Surface Defects on the Photocatalytic Activity of ZnO nanorods, *Sci Rep.*, **4**: 4596 (2014).

[31] Mesaros A., Toloman D., Nasui M., Mos R.B., Petrisor T., Vasile B.S., Surdu V.A., Perhaita I., Biris A., Pana O., A Valence States Approach for Luminescence Enhancement by Low Dopant Concentration in Eu Doped ZnO Nanoparticles, *Journal of Materials Science*, **50**(18): 6075-6086 (2015).

[32] Mosquera E., Rojas-Michea C., Morel M., Gracia F., Fuenzalida V., Zarate R.A., Zinc Oxide Nanoparticles with Incorporated Silver: Structural, Morphological, Optical and Vibrational Properties, *Applied Surface Science*, **347**: 561-568 (2015).

[33] Saaedi A., Yousefi R., Jamali-Sheini F., Zak A.K., Cheraghizade M., Mahmoudian M.R., Baghchesara M.A., Dezaki A.S., XPS Studies and Photocurrent Applications of Alkali-Metals-Doped ZnO Nanoparticles under Visible Illumination Conditions, *Physica E: Low-dimensional Systems and Nanostructures*, **79**: 113-118 (2016).

[34] Choi Y., Beak M., Yong K., Solar-Driven Hydrogen Evolution Using a $CuInS_2$/CdS/ZnO Heterostructure Nanowire Array as Anefficient Photoanode, *Nanoscale*, **6**(15): 8914-8918 (2014).

[35] Hadzic B., Romcevic N., Sibera D., Narkiewicz U., Kuryliszyn-Kudelska I., Dobrowolski W., Romcevic M., Laser Power Influence on Raman Spectra of ZnO(Co) Nanoparticles, *Journal of Physics and Chemistry of Solids*, **91**: 80-85 (2016).

[36] Das D., Mondal P., Photoluminescence Phenomena Prevailing in c-Axis Oriented Intrinsic ZnO Thin Films Preparedby RF Magnetron Sputtering, *RSC Advances*, **4**(67): 35735-35743 (2014).

[37] Shrama S.K., Saurakhiya N., Barthwal S., Kumar R., Sharma A., Tuning of Structural, Optical, and Magnetic Properties of Ultrathin and Thin ZnO Nanowire Arrays for Nano Device Applications, *Nanoscale Research Letters*, **122**(9): 1-17 (2014).

[38] Yang R.D., Tripathy S., Li Y., Sue H.-J., Photoluminescence and Micro-Raman Scattering in ZnO Nanoparticles: The Influence of Acetate Adsorption, *Chemical Physics Letters*, **411**(1-3): 150-154 (2005).